Nonlinear vortex modes in dual-core photonic crystal fiber couplers

José Ramón Salgueiro* and Francisco Santos

Departamento de Física Aplicada, Facultade de Ciencias, Universidade de Vigo, As Lagoas s/n, 32004 Ourense, Spain
**Corresponding author: jrs@uvigo.es*

Received May 29, 2009; revised October 5, 2009; accepted October 11, 2009; posted October 12, 2009 (Doc. ID 112122); published November 16, 2009

We study the different families of vortex-type modes that can exist in a photonic crystal fiber with two close defects forming a dual-core coupler and presenting the Kerr nonlinearity. Those complex modes bifurcate from the real double-dipole states leading to different states with different phase structures. When power is high enough, single- and double-vortex modes as well as combinations of vortex and fundamental modes arise. Also, families of discrete vortices formed by multipoles located inside the cores are found. We classify the different families, describe their nontrivial bifurcations, and study the stability of the states identifying different scenarios. © 2009 Optical Society of America

OCIS codes: 190.6135, 190.4370.

1. INTRODUCTION

In recent years, a lot of attention has been paid to photonic crystal fibers (PCFs) due to the interesting properties they present in contrast with the conventional optical fibers [1,2]. A PCF is a tubular structure of a substrate material with a periodic array of air holes running parallel to the optical axis and presenting a central defect. Among the properties that make these structures very interesting are the endlessly monomode character; i.e., they support only the fundamental mode regardless the wavelength for a very broad range of geometrical parameters, the flexibility of dispersion control that allows to bring the point of minimum dispersion to a desired wavelength only acting on the geometrical parameters, and the possibility to enhance and precisely design the birefringence. According to the type of the central defect there can be two different kinds of guiding mechanisms. When the core defect is made of a hole of different size or shape (*hollow* fibers), guiding properties rely on Bragg scattering which leads to the existence of bandgaps in the frequency spectrum. On the other hand, when the defect consists in a lack of some of the central holes, so that the fiber core is made of the substrate material (*solid core* fibers), the guiding is accomplished by the conventional total internal reflection mechanism due to the fact that the air holes in the cladding region make it to have a lower mean refractive index than the core.

The particular geometry of PCFs, constituting a system with discrete symmetry, makes them present a modal spectrum different from that of conventional fibers [3] not only because of the specific symmetry properties but also because discreteness induces limitations in the number of modes [4]. The possibility of making PCFs of a material presenting a nonlinear response to the optical field makes those structures very appropriate for all-optical processing, since nonlinear effects are enhanced due to the strong confinement of the field inside the fiber core. In this way, optical fibers are known to support different kinds of nonlinear modes in the form of fundamental solitons [5] and vortices [6]. Importantly, the structure of the PCF allows on to stabilize nonlinear modes that are unstable in conventional homogeneous media. In fact, the stabilization of spatial optical solitons when the PCF substrate presents a Kerr nonlinear response was numerically demonstrated [7,8], which are known to undergo spreading or collapse in homogeneous media.

As it concerns vortex solitons, i.e., optical fields presenting a phase dislocation point and an increasing phase from 0 to $2\pi\ell$ around the dislocation, ℓ being an integer named vorticity or winding number, they may present in nonlinear media either radial symmetry [6,9] or a multilobed structure in the form of clusters [10–13] made of fundamental solitons presenting the characteristic vortex phase structure. Vortex solitons and soliton clusters were found to be stable in PCFs under a power threshold [14,15]. In a similar context, two-dimensional solitons and vortices were stabilized using a periodic square lattice [16,17].

In this paper we carry out a study of the vortexlike modes in a nonlinear Kerr-type PCF with two defects (lack of two consecutive or close air holes). The fundamental solutions for this kind of dual-core PCFs were already studied [18] resulting in, along with the usual symmetric and antisymmetric modes, a new asymmetric mode appearing over a power threshold bifurcating from the symmetric one. This new state is the key for the all-optical switching operations since it is stable whereas the symmetric one turns unstable beyond the bifurcation point making possible the suppression of the coupling. This effect of destabilization of the original solution to form a stable asymmetric state is known as *spontaneous symmetry breaking* (SSB) and was already studied for two-component nonlinear systems with a superposed periodic lattice [19]. On the other hand, it is worth mentioning

that experimental results on applications using dual-core PCFs were already reported, as for instance velocity measuring [20] or nonlinear optical switching [21].

The solutions with a vortex in either one or two of the PCF cores are, in principle, expected to be modulationally stable under a power threshold due to the PCF structure though azimuthally unstable. Nevertheless, there is the possibility of modifying this kind of systems introducing elements to enhance the stability properties. In fact, vector systems with an additional incoherently coupled component have been demonstrated to be suitable for stabilizing vortices [22,23]. Also, particular interest has recently been devoted to nonlocal nonlinear media, where the nonlinear response at a particular position does not exclusively depend on the field at that point but also on the field in the surroundings. This kind of media supports stable vortices [24–26] and also other types of solitary waves carrying angular momentum, such as azimuthally modulated rotating singular optical beams or azimuthons [27], or multipole and spiraling solitons [28], as well as spiraling multivortices [29]. The possibility of using such media for the fabrication of PCFs or the generation of such nonlinear response by means of complementary techniques such as filling up the PCF holes with nonlinear liquids makes the consideration of this basic and simpler system a necessary previous step for the study of fields with phase structure in nonlinear PCF structures.

In Section 2 we will present the model used to describe the nonlinear fields with vorticity in the dual-core nonlinear PCF. In Section 3 we find, classify, and study the different families of solutions and their bifurcation schemes. Finally, in Section 4, we analyze the stability of the different families of solutions.

2. MODEL AND STATIONARY STATES

We consider a PCF made of a material with refractive index n_s and with the nonlinear Kerr response structured with a triangular network of air holes (index n_a). The lack of two of those consecutive or close holes constitutes two defects forming a dual-core coupler (see Fig. 1). The effective increase in the linear index inside the cores with respect to the surroundings makes the PCF device of the index-guiding or solid-core type. We choose the optical axis of the PCF in the direction Z (propagation direction), so that the triangular structure lies on the transversal plane (X,Y) and comes given by the function $W(X,Y)=n_a+\delta V(X,Y)$, where $\delta=n_s-n_a$ is the index difference and

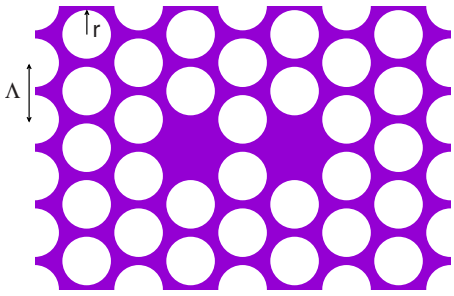

Fig. 1. (Color online) Sketch of the central part of the PCF with triangular structure and two close defects (double solid core) showing the basic parameters.

$V(X,Y)$ is a normalized function which takes the value $V=1$ in the substrate and the value $V=0$ inside the air holes. Thus, the optical scalar field $E(X,Y,Z)$ propagating inside the PCF along the Z direction can be modeled by the following nonlinear wave equation:

$$2ik\frac{\partial E}{\partial Z}+\nabla_\perp^2 E+2k^2[W(X,Y)+\gamma V(X,Y)|E|^2]E=0, \quad (1)$$

where $\nabla_\perp^2=\partial^2/\partial X^2+\partial^2/\partial Y^2$ is the Laplace operator, $k=2\pi/\lambda$ is the wavenumber related to the wavelength λ, and γ is a parameter describing the nonlinear Kerr response of the substrate. To further simplify the model we will choose $n_a=0$ without loss of generality. In fact, choosing a particular value for the base index n_a only has the effect of a shift in the modal spectrum. On the other hand, the parameters k, δ, and γ can be dropped from the equation by a proper rescaling of the spatial variables and the field. In fact, taking the new variables and field as $x=k\sqrt{2\delta}X$, $y=k\sqrt{2\delta}Y$, $z=k\delta Z$, and $U=\sqrt{\gamma/\delta}E$, the equation takes the following canonical form:

$$i\frac{\partial U}{\partial z}+\nabla_\perp^2 U+V(x,y)(1+|U|^2)U=0, \quad (2)$$

where the Laplace operator is now referred to the new spatial variables x and y.

We are interested in solutions which remain stationary along the propagation direction z, being of the form

$$U(x,y,z)=u(x,y)\exp(i\beta z), \quad (3)$$

where β is the propagation constant. Also, we are interested in solutions presenting phase dislocations (vortices) so that the phase performs a number of windings around the dislocation. In principle, we seek stationary solutions $u(x,y)$ with phase dislocations located at the center of each defect core, so that the phase increases from 0 to $2\pi\ell$ around any or both core centers, with ℓ being the vorticity or winding number. According to this, the function u describing the transversal amplitude of the stationary field should be a complex function. In this work we will focus on the simplest case of first-order vortices, considering $\ell=1$. Substituting Eq. (3) into Eq. (2) we come up with the following z-independent equation for the transversal field amplitude:

$$-\beta u+\nabla_\perp^2 u+V(x,y)(1+|u|^2)u=0. \quad (4)$$

Now considering the real and imaginary parts of u separately, $u=u_1+iu_2$, and substituting into Eq. (4) we obtain a system of two identical equations for u_1 and u_2,

$$-\beta u_i+\Delta_\perp u_i+V(1+u_1^2+u_2^2)u_i=0, \quad i=1,2. \quad (5)$$

Although both equations are identical, they are coupled by the nonlinear term and, consequently, the functions u_1 and u_2 representing real and imaginary parts of the field are in general different. The model is equivalent to the one describing a vector system where the two incoherently coupled components present the same propagation constant.

3. FAMILIES OF NONLINEAR MODES

We solved the system described by Eq. (5) numerically [30]. The nonlinearity makes solutions of Eq. (4) dependent on power, $P=\int(u_1^2+u_2^2)\mathrm{d}x\mathrm{d}y$, and there exist different families, each one described by a curve in the plane (β,P), which show different field amplitudes or phase configurations. Different kinds of symmetric and asymmetric solutions containing vortices in either one or both cores were found. There also exist first-order solutions without any phase structure which can also be symmetric or asymmetric and present the shape of double or single dipoles. In Subsections 3.A–3.C we will describe the different types of solutions classifying them in three main groups. First, we briefly examine the solutions without any vorticity. Second, we will pay attention to those solutions presenting a vortex centered at each of the cores. We will generically name these states *double vortices* (DVs) and will examine the different subfamilies according to the amplitude distribution (shape) and phase structure. Finally, we will study the high asymmetric solutions containing vortices that we name *asymmetric vortices* (AVs). They are composed of a vortex in one of the cores and a field distribution without any phase structure in the other core.

The power curves correspondent to the families we are studying are plotted in Fig. 2. The numerical calculations were carried out considering a PCF with a pitch (distance between closest hole centers) of $\Lambda=10$ and hole radius $r=4$. These particular values of the parameters, which lead to holes filling a large fraction of the fiber section, are necessary in order that the PCF supports the first excited modes (as is the case of vortices). Otherwise, the strong monomode character of PCFs would not allow the existence of modes except for the fundamental.

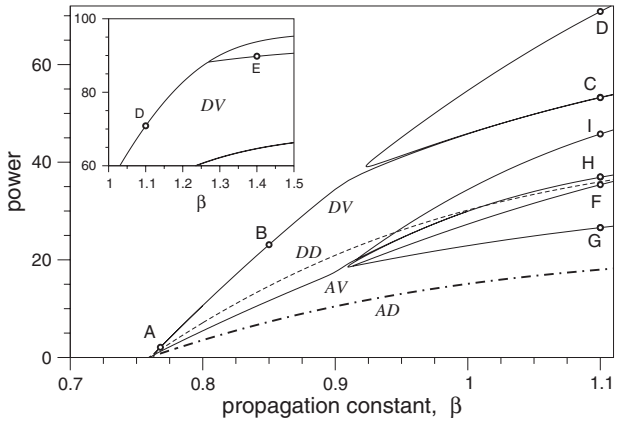

Fig. 2. Power versus propagation constant for the different families of vortexlike solutions (continuous curves), the double-dipole solutions (dashed curves), and the asymmetric dipoles (dashed-dotted curves). Big capital letters label points corresponding to the different examples shown in other figures below. The italic legends label the branches correspondent to the different types of solutions: double dipoles (DDs), asymmetric dipoles (ADs), DVs, and AVs. Beware that curves may actually constitute a bunch of close-together curves (not distinguished due to the scale of the figure) describing families of solutions with similar (though different) power. Inset: detail of the DV branch at higher power, where double-quadrupole solutions originate.

A. First-Order Solutions without Vorticity

If we focus on first-order solutions, the simplest stationary states are real-valued functions—with one of the components in Eq. (5) identically zero—in the form of double dipoles (DDs) which can present the four different configurations shown in Figs. 3(a)–3(d). Each configuration corresponds to a family of solutions on the power diagram represented in Fig. 2 as a dashed curve. There are actually four close-together lines (one for each solution type) as is shown in Fig. 4 (dashed lines) where the low power region of the diagram is zoomed.

In the linear limit ($P\to 0$) the four DDs are the unique first-order solutions possible since the double-core structure reduces the original discrete symmetry of the PCF, C_{6v}, into C_{2v}, and consequently they must remain invariant upon rotations of π radians or reflections with respect to the Cartesian coordinate axes. Besides, the states illustrated in Figs. 3(a) and 3(b) will be named *bounding* (b) and *antibounding* (a), respectively, regarding the molecular orbital theory, since they are characterized, respectively, by a high and low field density in the space between both cores. The other two families of solutions [Figs. 3(c) and 3(d)] will be named *parallel* (p) and *crossed* (x), respectively, due to the fact that both dipoles present same or opposite sign distribution. So, these four types of solutions will be denoted b, a, p, and x, respectively.

In a nonlinear regime, as a consequence of a SSB, there also exist asymmetric real-valued states in the form of DDs characterized by a different power on each of the cores, which can take the shape of single dipoles at high enough power. We name them *asymmetric dipoles*, and they can present one of the two shapes shown in Figs. 3(e) and 3(f) and bifurcate from the symmetric DDs at points O_5 and O_6 (see Fig. 4).

B. Symmetric Vortex Solutions

In the linear limit it is not possible to find vortexlike fields (with dislocations in one or two of the cores). In fact, as shown above, the reduction in symmetry induced by the dual-core structure makes the four DD solutions to be nondegenerate and consequently they cannot be combined to form a stationary state. When nonlinearity is present, however, it is possible to get stationary vortex solutions if real and imaginary parts are formed by DDs contributing with a different power; i.e., they are asymmetric with respect to the real and imaginary components. Examples of such stationary states with the shape

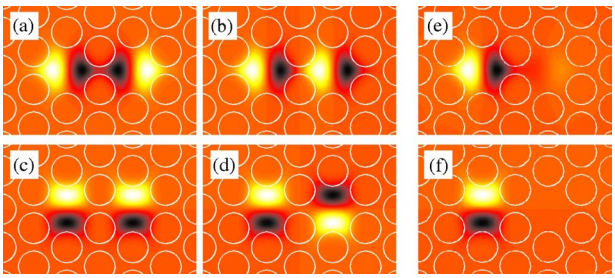

Fig. 3. (Color online) (a)–(d) Four DD states of a dual-core PCF for $\beta=0.8$: (a) bounding type (b), (b) antibounding (a), (c) parallel (p), (d) crossed (x). (e),(f) Two asymmetric dipoles (AD1 and AD2) that bifurcate from the DDs at points O_6 and O_7 (Fig. 4) and take the shape of single dipoles at high enough power.

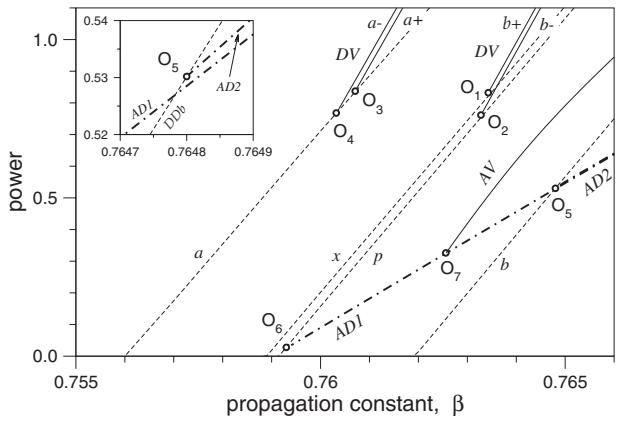

Fig. 4. Detail of the power curves for the low power regime. Dashed lines are the four DD families (b, a, p, and x stand for the bounding, antibounding, parallel, and crossed families, respectively). Points labeled O_1–O_4 are those from where the four DV families bifurcate [the four types bounding positive ($b+$), bounding negative ($b-$), antibounding positive ($a+$), and antibounding negative ($a-$) are indicated]. O_5 and O_6 are the bifurcation points for the two asymmetric DD families (labeled as AD1 and AD2 and plotted as dashed-dotted lines). O_7 is the bifurcation point for the AV. Inset: zoom of the region close to point O_5 to show that branches AD1 and AD2 are noncoincident.

of double-doughnut vortices are shown in Fig. 5. There are four types of DV solutions according to the type of DDs forming their real and imaginary parts; to be precise there are bounding and antiboundinglike solutions—we denote them as b and a—which have a bounding or antibounding DD, respectively, as one of the components, and each of those types can host two vortices of the same or the opposite vorticity, regarded as *positive* (+) and *negative* (−), respectively. Consequently, we denote the four possible DV solutions as $b+$, $b-$, $a+$, and $a-$. The amplitude and phase diagrams of Fig. 5 account for these four types of DVs.

The four different DV solutions are nondegenerated, so that the curve on the power diagram describing the DV family (Fig. 2) is actually formed by four close curves, each one correspondent to one of the types of DVs described above. They exist over a particular power threshold and bifurcate from the DDs at points O_1–O_4 as shown in the zoomed diagram of Fig. 4. The bounding-positive ($b+$) and bounding-negative ($b-$) DV families bifurcate

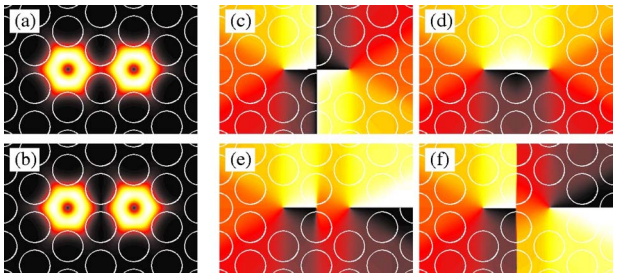

Fig. 5. (Color online) (a),(b) Intensity-level plots of two DV states for $\beta=0.85$ (point B in Fig. 2), one of the bounding type (a) and another of the antibounding type (b). (c)–(f) Phase patterns for each of the DV states correspondent to that point. Images (c) and (e) show the phase of the same vorticity states (+) and images (d) and (f) the phase of those with opposite vorticity (−), so that images (c)–(f) correspond to the states $b+$, $b-$, $a+$, and $a-$, respectively.

from the crossed and parallel DDs, respectively, whereas both antibounding solutions ($a+$ and $a-$) bifurcate from the antibounding DD. Close to the bifurcation points, power carried by real and imaginary components is increasingly different up to the point that one of them vanishes at the bifurcation point turning the state into the DD mode. An example of a DVs state of the $b+$ type close to the bifurcation point is shown in Fig. 6 (image A).

At higher powers we found DV solutions in the form of multipoles particularly with the shape of double tripoles and double quadrupoles (see examples in Fig. 6; cases C and E, respectively). The double-tripole solutions arise at moderate power and they are described in the power diagram (Fig. 2) by branches that originated from the main DV curves. The rise of solutions with a tripole shape is related to the symmetry of the PCF network. In fact, a single tripole (ST) presents the symmetry described by the group C_3 which is a subgroup of the C_{6v} symmetry group characteristic of the PCF. Nevertheless, the presence of the second core further limits the symmetry to C_{2v} and consequently only two different double tripoles can exist; those shown in Fig. 6 (images labeled C1 and C2). Again, the four combinations $b+$, $b-$, $a+$, and $a-$ are possible.

It is important to notice that the point where the double-tripole solutions start is not an actual bifurcation point. Instead, the branch of the doughnutlike vortices opens, so that both extremes join to one different double-tripole branch [see Figs. 2 and 7(a)]. As power increases, the lobes of the double-tripole solutions become increasingly narrower and their maximum amplitude increasingly larger, becoming independent of the PCF structure and so both curves merge. The transition between doughnutlike and tripole solutions is gradual and the absence of a proper bifurcation point is related to the fact that both double-tripole solutions are nondegenerated. In fact, the suppression of a bifurcation point due to an asymmetry that lifts a degeneration is already known in the context of asymmetric couplers [31]. We would like to remark at this point that this phenomenon is described in [19] as a *pseudobifurcation* in the context of a two-component system in a 2D square lattice. In that system, however, the asymmetry is not introduced by two defects in the lattice—the use of the coupled mode theory would not allow us to model the effect of the two side-by-side defects anyway. Instead, the asymmetry is introduced by a phase mismatch between the two lattices affecting each compo-

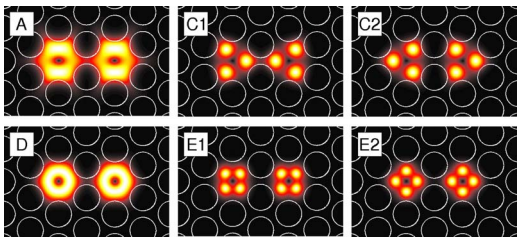

Fig. 6. (Color online) Some examples of DV states plotted as intensity-level images and correspondent to different branches in the power diagram. Two double-doughnut states (A, D)—one close to the bifurcation point (A)—two double tripoles (C1, C2), and two double quadrupoles (E1, E2) are shown. Labels correspond to points (A, C, D, and E) in Fig. 2.

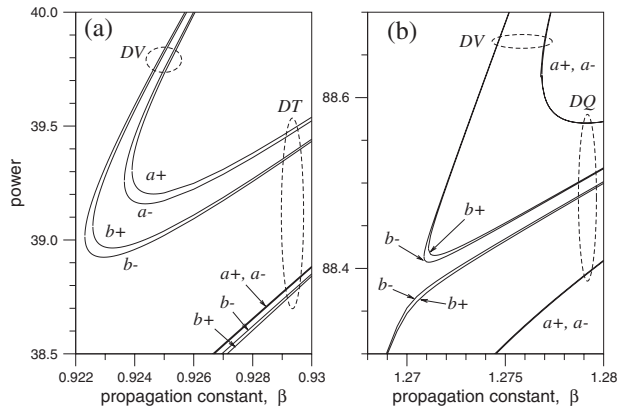

Fig. 7. (a) Detail of the power diagram at the junction where double-tripole branches (labeled DT) originate from the DV ones. Different curves correspondent to families of different phase structure are shown: bounding positive ($b+$), bounding negative ($b-$), antibounding positive ($a+$), and antibounding negative ($a-$). For the low branch lines corresponding to the families $a+$ and $a-$ are very close and not resolved at the scale of the plot. (b) Same for the junction point where double-quadrupole (DQ) solutions originate. Again curves corresponding to $a+$ and $a-$ are too close to be resolved.

nent, but the result is similar: the suppression of the bifurcation point.

For even higher powers, double quadrupoles exist and again they are described by branches joining to the main DV curves [see Fig. 2 (inset) and Fig. 7(b)]. In this case the original symmetry of a single-core quadrupole (C_{4v}) does not belong to the group of the PCF symmetry, although they have in common the symmetry of the subgroup C_{2v}. As in the case of the double tripoles, the double-core structure of the PCF imposes a C_{2v} symmetry and the solution types shown in Fig. 6 (E1 and E2) constitute the unique possibilities.

C. Asymmetric Solutions with Vorticity

We have also found asymmetric solutions in the form of single-core vortices (SVs) and combinations of a vortex in one of the cores and a fundamental field in the other [vortex-fundamental (VF)]. In Fig. 8 we present some examples to illustrate different kinds of configurations. The existence of symmetric DVs as well as SVs suggests the existence of asymmetric DVs that could be generated from the DVs via a SSB. Nevertheless, we were unable to find such solutions. A possible explanation for the lack of

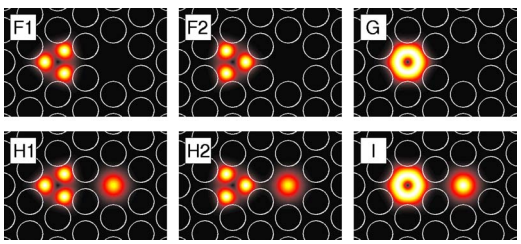

Fig. 8. (Color online) Some examples of single vortices and VF states with different shapes (shown as intensity plots): two types of STs (F1, F2), single doughnut (G), two types of TF states (H1, H2), and doughnut-fundamental state (I). Labels correspond to points in Fig. 2.

solutions with such a shape is the reduced symmetry of the dual-core system which makes the four DDs nondegenerated. Consequently, as commented above, the generation of a stationary vortex requires a specific power ratio between real and imaginary parts. Additionally, an asymmetric state also requires a specific ratio between power carried by each core and both conditions cannot be fulfilled simultaneously to form an asymmetric DV stationary solution. It is possible, however, to have a state with a vortex in one core and a field without phase structure in the other one.

At low power (see Fig. 2) there is a single curve of AVs describing the solutions of a vortex with a doughnut shape [of the form similar to the one shown in Fig. 8 (G)]. This curve bifurcates from one of the asymmetric DDs at point O_7 (see Fig. 4). Close to the bifurcation point, powers of real and imaginary parts become increasingly different up to the point (bifurcation) where one of them vanishes and the field takes the shape of an AD.

For higher power the asymmetric tripole solutions are found. In this case the junction region is much more complicated since several branches corresponding to several multipolar solutions appear (Fig. 8). On one hand, there are STs of two different shapes (images F1 and F2) which are nondegenerated due to the presence of the second core. On the other hand, there are also nondegenerated combinations of a tripole and a fundamental field [tripole-fundamental (TF)] also with two different shapes (images H1 and H2). These TF solutions, along with the VF with a doughnut vortex (image I), can also present two possible phase distributions that we name *bounding* (b) or *antibounding* (a) depending, respectively, on whether the fundamental field has the same or opposite sign as the closest lobe of the dipole forming the vortex. This means that the corresponding curves on the power diagram are actually formed by two close lines. In Fig. 9 we show the region of the junction point as a zoomed diagram representing all the lines describing the different family solutions

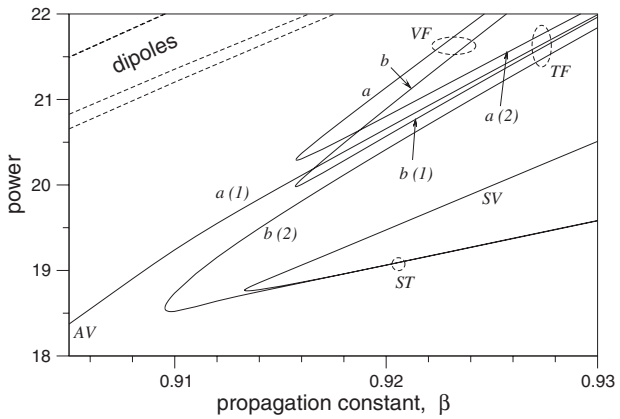

Fig. 9. Detail of the power diagram at the junction where different branches of ST and TF solutions originate from the asymmetric-vortex family. The shape of the different solutions is indicated with labels: single (doughnut) vortex (SV), ST, TF, and (doughnut) VF. Additionally, the type of solution according to the phase structure is also indicated with labels: bounding (b) and antibounding (a). The numbers in brackets indicate the type of solution according to symmetry criteria (cases F and H in Fig. 8).

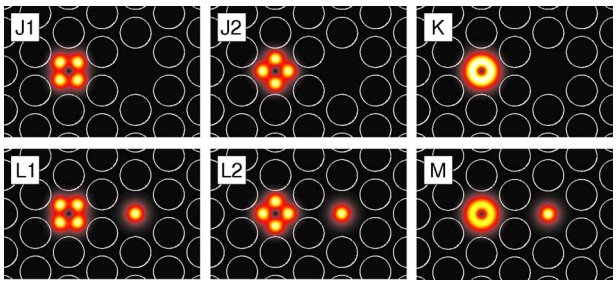

Fig. 10. (Color online) Examples of single vortices and VF states correspondent to families of the doughnut and quadrupole types. The two types of single quadrupoles (J1, J2) originate from the SV branch in Fig. 9 at higher power. The two types of quadrupole-fundamental states (L1, L2) originate from the VF branch at higher power. The doughnut-shaped single-vortex (K) and VF (M) are also examples related to a higher power.

and how they originate in a nontrivial way at the junction. Again, the breakage of symmetry induced by the dual-core structure prevents the existence of actual bifurcation points.

For higher powers, in a similar fashion as in the case of the DVs, the upper branches correspondent to the single-doughnut and doughnut-fundamental solutions go through new junction zones where single quadrupoles and combinations of quadrupoles and fundamental fields arise. Some examples are presented in Fig. 10. Again, the symmetry of the structure allows only two kinds of single quadrupoles (images J1 and J2) and two quadrupole-fundamental states (images L1 and L2). The latter ones can be of two types, bounding or antibounding.

4. STABILITY

We have checked the stability of the states of the different families by simulating their propagation using a standard beam propagation method. The main conclusion is the existence of two different scenarios. States characterized by a power over a threshold undergo collapse after a certain propagation distance. The higher the power the shorter the distance they evolve before collapsing as is shown in Fig. 11 cases (a) and (b) and (e) and (f) for DV and single-vortex states, respectively. Remarkably, this property is dependent on power density and not on the family under consideration. In fact, families with power distribution on both cores—DV and VF—present a collapse threshold about $P \sim 30$ while those families with power on a single core (single vortices) present a threshold around $P \sim 15.75$. In both cases the propagation constant at the threshold point is about $\beta \sim 0.88$. The power threshold is approximately at the point where the tripole solutions originate and consequently they undergo collapse upon propagation.

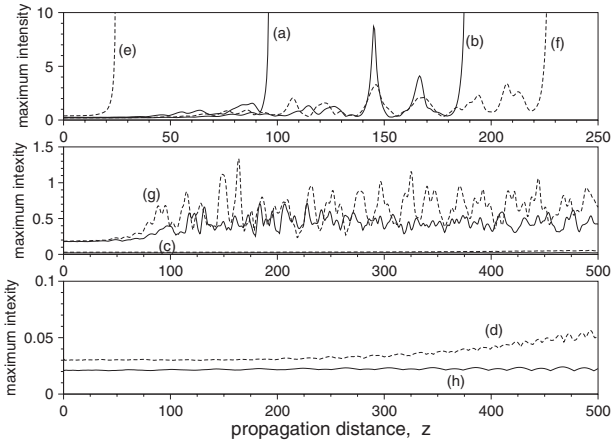

Fig. 11. Maximum intensity versus propagation distance for different double vortices (continuous curves) and single vortices (dashed curves). DV curves correspond to $P=34.4$ (a), $P=30.1$ (b), $P=27.9$ (c), and $P=5.8$ (d). Single-vortex simulations are for $P=27.3$ (e), $P=15.8$ (f), $P=15.1$ (g), and $P=2.76$ (h).

On the other hand, below the power threshold, the modes do not develop collapse and the PCF structure prevents them to spread out as in a bulk Kerr medium. Nevertheless, after a distance they develop the azimuthal instability so that the vortices break into fundamental solitons that remain spinning inside the PCF core. The distance for this breakup to occur depends on power, so that the lower the power the longest distance they survive as shown in Fig. 11 cases (c) and (d) and (g) and (h). For low powers (close to the linear limit) the distance before the breakup can be quite long.

Since the stationary states for a reasonable nonlinear regime are unstable, since they collapse or at least develop the azimuthal instability, an interesting further step is to seek ways to enhance the stability properties of the medium, as considering vectorial systems of incoherently coupled components or using media with nonlocal nonlinearities. Anyway, the study of the present system, due to the simplicity of the model, constitutes a necessary previous step for the study of vortices in dual-core PCFs.

5. CONCLUSIONS

In this work we have studied and classified the different stationary nonlinear vortex-type families of solutions in a PCF with two consecutive defects constituting a dual-core nonlinear coupler. We found solutions in the form of DVs with shapes of double doughnut, double tripole, and double quadrupole. Additionally, asymmetric solutions in the form of single vortices (located in one of the cores) and combination of vortices and fundamental states, also with doughnut, tripole, and quadrupole shapes, were also calculated. The power diagram with the different bifurcations and junction points was obtained and the different solution families were classified. Finally, we presented a stability study determining different instability scenarios.

ACKNOWLEDGMENTS

The authors thank Yuri Kivshar from The Australian National University for the very useful discussions and suggestions. This work was supported by the Ministerio de Ciencia e Innovación of Spain through the Acción Complementaria Internacional grant PCI2006-A7-0561, project MAT2008-06870, and the Ramón y Cajal contract granted to J. R. Salgueiro, and also by Xunta de Galicia, Spain through project PGIDIT06PXIB239155PR.

REFERENCES

1. Ph. Russell, "Photonic crystals fibers," Science **299**, 358–562 (2003).
2. J. C. Knight, "Photonic crystals fibers," Nature **424**, 847–851 (2003).
3. A. Ferrando, E. Silvestre, J. J. Miret, and P. Andrés, "Vector description of higher-order modes in photonic crystal fibers," J. Opt. Soc. Am. A Opt. Image Sci. Vis. **17**, 1333–1340 (2000).
4. A. Ferrando, M. Zacarés, and M. A. García-March, "Vorticity cutoff in nonlinear photonic crystals," Phys. Rev. Lett. **95**, 043901 (2005).
5. Yu. S. Kivshar and G. P. Agrawal, *Optical Solitons: From Fibers to Photonic Crystals* (Academic, 2003).
6. A. S. Desyatnikov, Yu. S. Kivshar, and L. Torner, in *Progress in Optics*, E. Wolf, ed. (North-Holland, 2005), Vol. 47.
7. A. Ferrando, M. Zacarés, P. Fernández de Córdoba, D. Binosi, and J. A. Monsoriu, "Spatial soliton formation in photonic crystal fibers," Opt. Express **11**, 452–459 (2003).
8. J. R. Salgueiro, Yu. S. Kivshar, D. E. Pelinovski, V. Simón, and H. Michinel, "Spatial vector solitons in nonlinear photonic crystal fibers," Stud. Appl. Math. **115**, 157–171 (2005).
9. V. I. Kruglov and R. A. Vlasov, "Spiral self-trapping propagation of optical beams in media with cubic nonlinearity," Phys. Lett. A **111**, 401–404 (1985).
10. A. S. Desyatnikov and Yu. S. Kivshar, "Rotating optical soliton clusters," Phys. Rev. Lett. **88**, 053901 (2002).
11. Y. V. Kartashov, L. C. Crasovan, D. Mihalache, and L. Torner, "Robust propagation of two-color soliton clusters supported by competing nonlinearities," Phys. Rev. Lett. **89**, 273902 (2002).
12. A. Desyatnikov and Yu. Kivshar, "Spatial optical solitons and soliton clusters carrying an angular momentum," J. Opt. B: Quantum Semiclassical Opt. **4**, S58–S64 (2002).
13. D. Mihalache, D. Mazilu, L. C. Crasovan, B. A. Malomed, F. Lederer, and L. Torner, "Robust soliton clusters in media with competing cubic and quintic nonlinearities," Phys. Rev. E **68**, 046612 (2003).
14. A. Ferrando, M. Zacarés, P. Fernández de Córdoba, D. Binosi, and J. A. Monsoriu, "Vortex solitons in photonic crystal fibers," Opt. Express **12**, 817–822 (2004).
15. J. R. Salgueiro and Yu. S. Kivshar, "Optical vortex solitons and soliton clusters in photonic crystal fibres," Eur. Phys. J. Spec. Top. **173**, 281–288 (2009).
16. P. Xie, Z. Zhang, and X. Zhang, "Gap solitons and soliton trains in finite-sized two-dimensional periodic and quasi-periodic photonic crystals," Phys. Rev. E **67**, 026607 (2003).
17. B. B. Baizakov, B. A. Malomed, and M. Salerno, "Multidimensional solitons in periodic potentials," Europhys. Lett. **63**, 642–648 (2003).
18. J. R. Salgueiro and Yu. S. Kivshar, "Nonlinear dual-core photonic crystal fiber couplers," Opt. Lett. **30**, 1858–1860 (2005).
19. A. Gubeskys and B. A. Malomed, "Spontaneous soliton symmetry breaking in two-dimensional coupled Bose–Einstein condensates supported by optical lattices," Phys. Rev. A **76**, 043623 (2007).
20. W. N. MacPherson, J. D. C. Jones, B. J. Mangan, J. C. Knight, and P. D. J. Russell, "Two-core photonic crystal fibre for Doppler difference velocimetry," Opt. Commun. **223**, 375–380 (2003).
21. A. Betlej, S. Suntsov, K. G. Makris, L. Jankovic, D. N. Christodoulides, G. I. Stegeman, J. Fini, R. T. Bise, and D. J. DiGiovanni, "All-optical switching and multifrequency generation in a dual-core photonic crystal fiber," Opt. Lett. **31**, 1480–1482 (2006).
22. J. Yang and D. E. Pelinovsky, "Stable vortex and dipole vector solitons in a saturable nonlinear medium," Phys. Rev. E **67**, 016608 (2003).
23. J. R. Salgueiro and Yu. S. Kivshar, "Single- and double-vortex vector solitons in self-focusing nonlinear media," Phys. Rev. E **70**, 056613 (2004).
24. A. I. Yakimenko, Y. A. Zaliznyak, and Yu. Kivshar, "Stable vortex solitons in nonlocal self-focusing nonlinear media," Phys. Rev. E **71**, 065603 (2005).
25. D. Briedis, D. E. Petersen, D. Edmundson, W. Krolikowski, and O. Bang, "Ring vortex solitons in nonlocal nonlinear media," Opt. Express **13**, 435–443 (2005).
26. A. A. Minzoni, N. F. Smyth, A. L. Worthy, and Yu. S. Kivshar, "Stabilization of vortex solitons in nonlocal nonlinear media," Phys. Rev. A **76**, 063803 (2007).
27. S. Lopez-Aguayo, A. S. Desyatnikov, and Yu. S. Kivshar, "Azimuthons in nonlocal nonlinear media," Opt. Express **14**, 7903–7908 (2006).
28. D. Buccoliero, S. López-Aguayo, S. Skupin, A. S. Desyatnikov, O. Bang, W. Krolikowski, and Yu. S. Kivshar, "Spiraling solitons and multipole localized modes in nonlocal nonlinear media," Physica B **394**, 351–356 (2007).
29. D. Buccoliero, A. S. Desyatnikov, W. Krolikowski, and Yu. S. Kivshar, "Spiraling multivortex solitons in nonlocal nonlinear media," Opt. Lett. **33**, 198–200 (2008).
30. J. R. Salgueiro, D. Olivieri, and H. Michinel, "Computation of linear and nonlinear stationary states of photonic structures using modern iterative solvers," Opt. Quantum Electron. **39**, 239–260 (2007).
31. N. N. Akhmediev and A. Ankiewicz, *Solitons* (Chapman and Hall, 1997).